THE Nd–Sr ISOTOPIC CORRELATION IN MANTLE MATERIALS AND GEODYNAMIC CONSEQUENCES

CLAUDE J. ALLEGRE, DALILA BEN OTHMAN, MIREILLE POLVE and PIERRE RICHARD

Laboratoire de Géochimie et Cosmochimie (LA 196), Département des Sciences de la Terre (Université Paris VII), Institut de Physique du Globe (Université Paris VI), 4 Place Jussieu, 75005 Paris (France) *

The neodymium–strontium isotopic correlation observed in most of the Earth mantle materials is evaluated by means of direct modelling. Several geochemical models are quantitatively developed to explain the observations. The main results of this modelling are that such a correlation is not geochemically trivial and that it corresponds to specific conditions in chemical fractionation. These specific conditions seem to be satisfied by solid–liquid partitioning in magmatic conditions. The discussion of the experimental data supports a continuous convecting-magmatic fractionation model for a large proportion of the mantle.

1. Introduction

The recent discovery of the heterogeneity of the Earth's mantle with respect to neodymium isotopic composition (Richard et al., 1976; De Paolo and Wasserburg, 1976a and b, 1977; O'Nions et al., 1977) has led to the detection of an important natural relationship, the inverse correlation between strontium and neodymium isotopes in recent basalts. This correlation, first suggested by Richard et al. (1976), has been convincingly documented by De Paolo and Wasserburg (1977) and by O'Nions et al. (1977). The last-named authors have accumulated an enormous number of data (see Hawkesworth et al., 1977). However this remarkable relationship has not been quantitatively explained or exploited, and it is the purpose of the present paper to do so.

2. Neodymium–strontium isotopic relationship in basalts

Before discussing the quantitative models, we will establish clearly the parameters of the Nd–Sr isotopic

relationship. All the data available in the literature for oceanic basalts, recalculated and normalized to a common reference value, are grouped in Table I. The results for continental flood basalts will be discussed separately, because of the high possibility of contamination by the continental crust (see below). The inverse correlation between the $^{143}Nd/^{144}Nd$ and $^{87}Sr/^{86}Sr$ ratios (see Fig. 1) can be calculated using a least-squares program with independent errors, giving the following parameters:

$$(^{143}Nd/^{144}Nd) = a(^{87}Sr/^{86}Sr) + b$$

where

$$a = -0.2450 \pm 0.0214 \ (\sigma); \quad \text{and}$$

$$b = \ 0.6845 \pm 0.0149 \ (\sigma)$$

Using this straight line, we can, following the work of De Paolo and Wasserburg (1977) determine the $^{87}Sr/^{86}Sr$ value corresponding to the present-day $^{143}Nd/^{144}Nd$ value for the "chondritic" mantle. The word "chondritic" refers only to the relative REE distribution and not to the absolute amounts of REE. This REE distribution is common to many meteorites

TABLE I

Data on oceanic basalts available from the literature

Samples	$^{143}Nd/^{144}Nd$ *	$(\epsilon_{Nd})_{PI}$	$^{147}Sm/^{144}Nd$	$^{87}Sr/^{86}Sr$	$(\epsilon_{Sr})_{PI}$	Author **
Mid ocean ridge basalts						
VG 295 thol. M.A.R. 22.5°N; 45°W	0.51238 ± 5	+10.6 ± 0.9	–	0.70226 ± 6	−36.0 ± 0.8	DPW
TD 10 thol. M.A.R. Gibbs zone	0.51233 ± 7	+9.7 ± 1.4	–	0.7033	−21.3	RSA
T 87 thol. M.A.R. 25°N	0.51229 ± 7	+8.9 ± 1.4	–	0.70290	−27.0	RSA
T 89 thol. M.A.R. 25°N	0.51241 ± 9	+11.2 ± 1.8	–	0.70264	−30.6	RSA
111327 thol. M.A.R. 11°N	0.51233 ± 3	+9.7 ± 0.5	0.217	0.70249 ± 4	−32.8 ± 0.5	OHE
AD 3-3 thol. M.A.R. 6°S	0.51250 ± 2	+13.0 ± 0.4	0.217	0.70230 ± 4	−35.5 ± 0.5	OHE
CH 31 thol. M.A.R. Famous area	0.51238 ± 9	+10.6 ± 1.8	–	0.70284 ± 5	−27.8 ± 0.5	RSA
ARP 74 thol. M.A.R. Famous area	0.51223 ± 3	+7.7 ± 0.6	–	0.7035	−18.4	RSA
OSG 3 thol. M.A.R. Reykjanes r.	0.51234 ± 3	+9.9 ± 0.5	0.236	0.70298 ± 3	−25.8 ± 0.4	OHE
OSG 24 thol. M.A.R. Reykjanes r.	0.51224 ± 3	+7.8 ± 0.5	0.191	0.70316 ± 4	−23.3 ± 0.5	OHE
PD1P thol. East Pac. Rise	0.51237 ± 4	+10.4 ± 0.8	–	0.70248 ± 10	−32.9 ± 1.5	RSA
332 A 8-2	0.51230 ± 2	+9.1 ± 0.4	0.155	0.70302 ± 4	−25.3 ± 0.5	OHE
17-1 DSDP leg 37	0.51231 ± 2	+9.3 ± 0.4	0.163	0.70300 ± 4	−25.5 ± 0.5	OHE
25-1 37°N	0.51236 ± 4	+10.3 ± 0.8	0.215	0.70287 ± 4	−27.4 ± 0.5	OHE
35-3 33°W	0.51231 ± 2	+9.3 ± 0.4	0.215	0.70308 ± 4	−24.4 ± 0.5	OHE
Oceanic island basalts						
NAL 27 thol. Iceland	0.51228 ± 7	+8.7 ± 1.4	–	0.70304 ± 5	−25.0 ± 0.7	RSA
R 14 thol. Iceland	0.51223 ± 3	+7.8 ± 0.5	0.191	0.70304 ± 3	−25.0 ± 0.4	OHE
R 40 thol. Iceland	0.51224 ± 3	+7.9 ± 0.5	0.186	0.70321 ± 4	−22.6 ± 0.5	OHE
TH 16 thol. Iceland	0.51223 ± 3	+7.7 ± 0.5	0.185	0.70315 ± 5	−23.4 ± 0.7	OHE
Th 29 thol. Iceland	0.51223 ± 3	+7.7 ± 0.5	0.264	0.70291 ± 4	−26.8 ± 0.5	OHE
N 30 thol. Iceland	0.51224 ± 2	+7.9 ± 0.4	0.186	0.70329 ± 5	−21.4 ± 0.7	OHE
T 14 thol. Iceland	0.51214 ± 3	+5.6 ± 0.5	0.124	0.70363 ± 5	−16.6 ± 0.8	OHE

Sample						
SNS 7 alk. b. Iceland	0.51215 ± 2	+6.1 ± 0.4	0.129	0.70341 ± 5	−19.7 ± 0.7	OHE
SNS 25 alk. b. Iceland	0.51217 ± 2	+6.5 ± 0.4	0.132	0.70340 ± 6	−19.9 ± 0.8	OHE
T4 alk. b. Terceira Açores	0.51215 ± 4	+6.1 ± 0.8	—	0.70347 ± 8	−18.9 ± 1.1	RSA
S4 alk. b. Sta Maria Açores	0.51210 ± 12	+5.2 ± 2.4	—	0.70360 ± 10	−17.0 ± 1.5	RSA
A 15221 trach. Ascension Island	0.51226 ± 3	+8.3 ± 0.5	0.138	0.70287 ± 7	−27.4 ± 1.0	OHE
A 15085 hawaiite Ascension Island	0.51218 ± 2	+6.7 ± 0.4	0.143	0.70282 ± 6	−28.1 ± 0.8	OHE
A 17308 mugearite Ascension Island	0.51220 ± 2	+7.1 ± 0.4	0.120	0.70281 ± 5	−28.2 ± 0.7	OHE
A 15176 alk. b. Ascension Island	0.51224 ± 3	+7.9 ± 0.5	0.143	0.70276 ± 7	−28.9 ± 1.0	OHE
T 369 trachy b. Tristan da Cunha	0.51171 ± 3	−2.4 ± 0.5	0.114	0.70505 ± 12	+3.5 ± 0.5	OHE
T 617 trach. and Tristan da Cunha	0.51176 ± 3	−1.5 ± 0.5	0.103	0.70517 ± 6	+5.2 ± 0.4	OHE
BV 1 trachyte Bouvet Islands	0.51206 ± 3	+4.4 ± 0.5	0.140	0.70365 ± 3	−16.3 ± 0.4	OHE
BV 2 trachyte Bouvet Islands	0.51203 ± 2	+3.8 ± 0.4	0.138	0.70370 ± 4	−15.6 ± 0.5	OHE
BV 3 basalt Bouvet Islands	0.51205 ± 3	+4.2 ± 0.6	0.150	0.70367 ± 5	−16.0 ± 0.7	OHE
BV 5 basalt Bouvet Islands	0.51206 ± 2	+4.4 ± 0.4	0.177	0.70374 ± 3	−15.0 ± 0.4	OHE
HN1 neph. Hawaiian Islands	0.51221 ± 3	+7.3 ± 0.6	0.123	0.70320 ± 8	−22.7 ± 1.1	DPW
HT 1 thol. Hawaiian Islands	0.51188 ± 3	+0.8 ± 0.6	0.159	0.70403 ± 6	−10.9 ± 0.8	DPW
HA 5 thol. Hawaiian Islands	0.51210 ± 3	+5.2 ± 0.5	0.183	0.70331 ± 4	−21.1 ± 0.5	OHE
T 10 ol. b. Hawaiian Islands	0.51209 ± 2	+5.0 ± 0.4	0.177	0.70380 ± 3	−14.2 ± 0.4	OHE
HA 4 hawaiite Hawaiian Islands	0.51222 ± 2	+7.4 ± 0.4	0.139	0.70384 ± 4	−13.6 ± 0.5	OHE
T 14 andesite Hawaiian Islands	0.51220 ± 3	+7.1 ± 0.5	0.137	0.70352 ± 5	−18.2 ± 0.7	OHE
T 17 ol. b. Hawaiian Islands	0.51217 ± 2	+6.5 ± 0.4	0.150	0.70366 ± 5	−16.2 ± 0.7	OHE
HA 2 alk. b. Hawaiian Islands	0.51214 ± 2	+5.9 ± 0.4	0.145	0.70361 ± 5	−16.9 ± 0.7	OHE
T 4 ol. b Hawaiian Islands	0.51220 ± 4	+7.1 ± 0.8	0.157	0.70353 ± 4	−18.0 ± 0.5	OHE
HA 7 trachyte Hawaiian Islands	0.51209 ± 2	+5.0 ± 0.4	0.121	0.70340 ± 5	−19.9 ± 0.7	OHE
T 20 neph. b. Hawaiian Islands	0.51228 ± 3	+8.7 ± 0.5	0.100	0.70316 ± 3	−23.3 ± 0.4	OHE
HA 8 neph. b. Hawaiian Islands	0.51229 ± 3	+8.1 ± 0.5	0.131	0.70351 ± 4	−18.3 ± 0.5	OHE

* Normalized to $^{146}Nd/^{144}Nd = 0.724118$.

** Authors are abbreviated as follows: DPW, De Paolo−Wasserburg (1976−1977); OHE, O'Nions−Hamilton−Evensen (1977); and RSA, Richard−Shimizu−Allègre (1976).
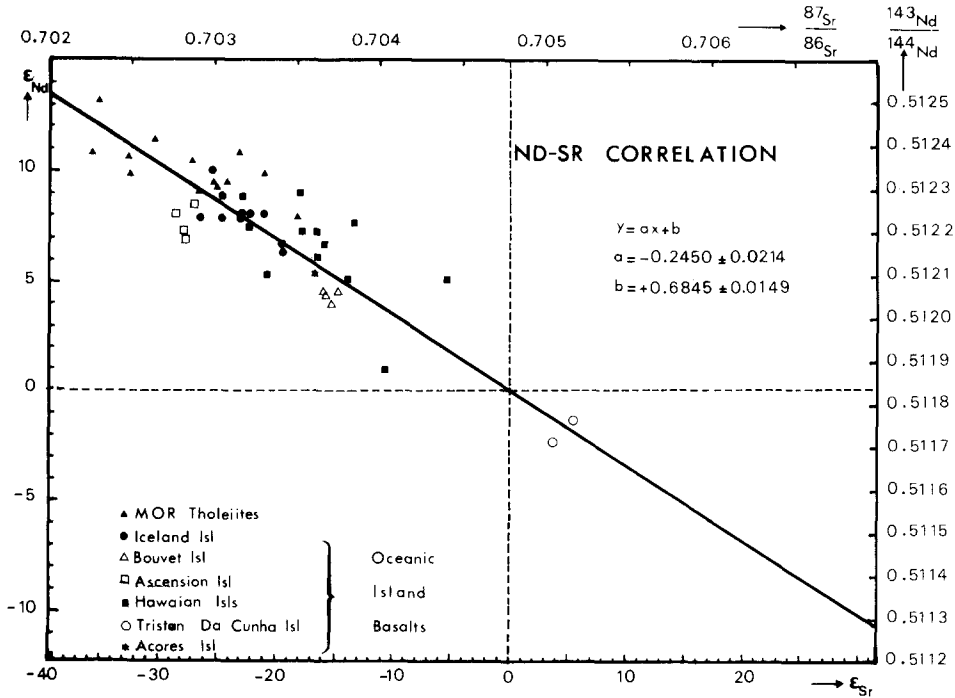
Fig. 1. Correlation diagram between the isotopic ratios of strontium and neodymium in volcanic material as established by Richard et al. (1976), De Paolo and Wasserburg (1976a), and O'Nions et al. (1977), corresponding to the compilation in Table I. The best line has been calculated by a least-squares program with independent errors. The graduation is given in both ratio and ϵ notation as discussed in the text.
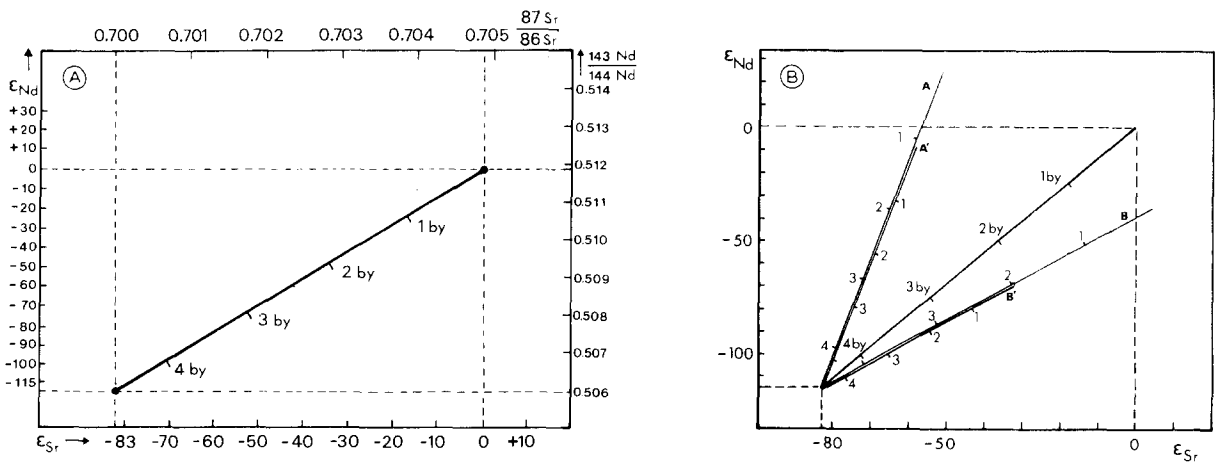

Fig. 2. Evolution of closed reservoirs through geological time in the (ϵ_{Nd}, ϵ_{Sr}) diagram.
(a) Shows the evolution corresponding to the real parameter of a terrestrial closed reservoir corresponding to a planetary Sm/Nd ratio and an initial ($^{143}Nd/^{144}Nd$) ratio corresponding to Juvinas (Lugmair, 1976).
(b) is a hypothetical set of reservoir evolutions corresponding to different sets of ρ/μ ratios and ρ and μ absolute values. Curves (A and A') have, respectively, $\rho/\mu = 0.45$, $\rho_1 = 0.108$, and $\rho_1' = 0.086$. Curves (B and B') have, respectively, $\rho/\mu = 0.075$, $\rho_2 = 0.324$, and $\rho_2' = 0.184$.

(including carbonaceous, differentiated and ordinary chondrites) and is assumed to be the initial distribution for all planetary objects, including the Earth and the Moon. The word "chondritic" is thus somewhat ambiguous because it implies the idea of a chondritic model for the Earth. Therefore, we propose to call these values "planetary values". To calculate $^{143}Nd/^{144}Nd$ ratios for a "planetary" material, two sources of data are available.

Since achondrites have an Sm/Nd ratio which is relatively unfractionated compared to that of their parent body, and a time of formation very close to that of the Earth, the present-day value of the $^{143}Nd/^{144}Nd$ ratio closely approximates the planetary value. The only data reported are those on the Juvinas eucrite (Lugmair, 1974; Lugmair et al., 1975, 1976), which give a $^{143}Nd/^{144}Nd$ ratio of 0.511836 ± 0.00004 (2σ). The Sm/Nd ratio is equal to 0.308, corresponding to a $^{147}Sm/^{144}Nd$ ratio of 0.1936.

Using the correlation diagram we estimate the present-day planetary value of $^{87}Sr/^{86}Sr$ as 0.70478 ± 0.00008 (2σ *). This value corresponds to a closed-system reservoir from the beginning of the Earth to the present day, with an Rb/Sr ratio of 0.031 (corresponding to an $^{87}Rb/^{86}Sr$ ratio of 0.090), an initial $^{87}Sr/^{86}Sr$ ratio of 0.69899, and the values $\lambda_{Nd} = (6.54 \pm 0.08) \, 10^{-12} \, Y^{-1}$, and $\lambda_{Sr} = (1.42 \pm 0.01) \, 10^{-11} \, Y^{-1}$ (see Fig. 2a).

We can now transform the diagram using the ϵ notation. Following the notation proposed twenty years ago by Epstein for the oxygen isotopic ratio, we can express our results in terms of a deviation relative to a standard, as suggested by Lugmair et al. (1976) and by De Paolo and Wasserburg (1976a). We will take as the standard the present-day planetary values determined above, namely, $(^{143}Nd/^{144}Nd)_{Pl} = 0.51184$, and $(^{87}Sr/^{86}Sr)_{Pl} = 0.7048$. The ϵ values are then calculated using the formulae:

$$\epsilon_{Nd} = \frac{[(^{143}Nd/^{144}Nd)_m - (^{143}Nd/^{144}Nd)_{Pl}]}{(^{143}Nd/^{144}Nd)_{Pl}} \cdot 10^4$$

$$\epsilon_{Sr} = \frac{[(^{87}Sr/^{86}Sr)_m - (^{87}Sr/^{86}Sr)_{Pl}]}{(^{87}Sr/^{86}Sr)_{Pl}} \cdot 10^4$$

* Assuming that the error is only due to the uncertainty in the planetary value of $^{143}Nd/^{144}Nd$.

where subscript (m) refers to the measured values and subscript (Pl) to the planetary values.

We can now consider again the correlation diagram in (ϵ_{Sr}, ϵ_{Nd}) notation. In such a diagram, the (0, 0) point represents the present-day values of ϵ_{Nd}, ϵ_{Sr} for the Earth, beginning with planetary values for REE and Sr, and growing in a closed system: the equation of the correlation line is now:

$$\epsilon_{Nd} = -0.3374\epsilon_{Sr}$$

Note that all oceanic basalts which represent samples from the mantle uncontaminated by the radiogenic crust are in the domain (+, −) which means $\epsilon_{Nd} > 0$, $\epsilon_{Sr} < 0$. If the whole Earth started with a truly planetary distribution, we should find in the Earth a reservoir, which balances the oceanic domain with respect to Nd and Sr, and which has a (−, +) characteristic. Such a reservoir, which cannot be the upper mantle under the oceans, may be under the continents, in the continental lithosphere itself, or in the lower non-convective mantle.

It should also be noted that the distribution of points is continuous: the mid-oceanic-ridge basalts have higher ϵ_{Nd} and lower ϵ_{Sr} values than do island basalts, but there is a continuous transition rather than a clear gap between the two families. In fact, such a continuity is also observed for the lead isotopes and has important consequences on the dynamic evolution of the Earth: for instance, the continuity is more in favour of a continuous convective process rather than other more catastrophic models.

3. Quantitative models in the (Nd, Sr) isotopic evolution diagram

3.1. Simple closed-system evolution model

We consider a reservoir which had, at the time T_0

$$(^{143}Nd/^{144}Nd)_{T_0} = \alpha_0 \; ; \qquad (^{87}Sr/^{86}Sr)_{T_0} = \beta_0$$

In a closed system, the growth of Nd and Sr isotopic compositions on going from T_0 to T are, respectively:

$$\alpha_T = \alpha_0 + (^{147}Sm/^{144}Nd)/[\exp(\lambda T_0) - \exp(\lambda T)]$$

$$\beta_T = \beta_0 + (^{87}Rb/^{86}Sr)/[\exp(\lambda' T_0) - \exp(\lambda' T)]$$

Writing $^{147}Sm/^{144}Nd$ as μ, $^{87}Rb/^{86}Sr$ as ρ, and assuming that λ, λ' and T_0 are such that we can expand α and β in a first-order Taylor series:

$$\alpha_T = \alpha_0 + \mu\lambda(T_0 - T); \qquad \beta_T = \beta_0 + \rho\lambda'(T_0 - T)$$

The evolution curve with time in an (α, β) diagram is a straight line passing through α_0 and β_0

$$\beta_T - \beta_0 = (\rho\lambda'/\mu\lambda)(\alpha_T - \alpha_0) \qquad (1)$$

with a slope of $\rho\lambda'/\mu\lambda$ (see Fig. 2b).

If we consider that T_0 is the age of the Earth and use the ϵ notation previously defined, then at time T

$$(\epsilon_{Nd})_T = [\alpha_T - (\alpha_0 + \mu_{Pl}\lambda T_0)] \cdot 10^4/(\alpha_0 + \mu_{Pl}\lambda T_0)$$
$$(2a)$$

$$(\epsilon_{Sr})_T = [\beta_T - (\beta_0 + \rho_{Pl}\lambda' T_0)] \cdot 10^4/(\beta_0 + \rho_{Pl}\lambda' T_0)$$
$$(2b)$$

Writing $\alpha_0 + \mu_{Pl}\lambda T_0 = \alpha_{Pl}$, and $\beta_0 + \rho_{Pl}\lambda' T_0 = \beta_{Pl}$, eqs. 2a and 2b give

$$[(\epsilon_{Nd})_T \cdot 10^{-4} + 1]\alpha_{Pl} = \alpha_T ; \qquad \text{and}$$

$$[(\epsilon_{Sr})_T \cdot 10^{-4} + 1]\beta_{Pl} = \beta_T$$

In particular:

$$\alpha_0 = [(\epsilon_{Nd})_{T_0} \cdot 10^{-4} + 1]\alpha_{Pl} ; \qquad \text{and}$$

$$\beta_0 = [(\epsilon_{Sr})_{T_0} \cdot 10^{-4} + 1]\beta_{Pl}$$

Then, eq. 1 can be re-written:

$$[(\epsilon_{Sr})_T - (\epsilon_{Sr})_{T_0}]\beta_{Pl} = (\rho\lambda'\alpha_{Pl}/\mu\lambda)[(\epsilon_{Nd})_T - (\epsilon_{Nd})_{T_0}]$$

so that

$$(\epsilon_{Sr})_T = (\rho\lambda'\alpha_{Pl}/\mu\lambda\beta_{Pl})(\epsilon_{Nd})_T - (\rho\lambda'\alpha_{Pl}/\mu\lambda\beta_{Pl})(\epsilon_{Nd})_{T_0}$$
$$+ (\epsilon_{Sr})_{T_0}$$

The evolution line is a straight line with a slope $\rho\lambda'\alpha_{Pl}/\mu\lambda\beta_{Pl}$, and passing through the point (α_0, β_0). We notice that if the slope of this line depends only on the μ/ρ value, the time graduation on the line depends on the absolute values of μ and ρ. We remark also that for each time T there corresponds a linear correlation between ϵ_{Nd} and ϵ_{Sr} passing through the point (α_T, β_T) with a slope parallel to the present $(\epsilon_{Nd}, \epsilon_{Sr})$ line (Fig. 3).
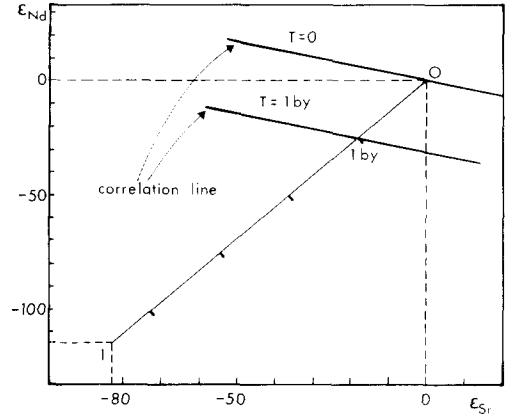

Fig. 3. Correlation lines in the past. If we now consider the plot of initial ratios of Nd and Sr for 1-b.y. rocks, these results will fall on the correlation line after 1 b.y. If we plot the measured ratios they will fall on the $T = 0$ correlation line. Of course, such a case will only hold if the subsystem follows the requirements developed in the text.

3.2. Single-episode fractionation model

In this model we suppose that at T_0, the age of the Earth, the mantle had planetary values. Then, at a certain time T_1, the mantle suffered an episode of chemical fractionation, particularly between Sm and Nd, Rb and Sr. Geodynamically, such an event can be differentiation of the core, or the differentiation of the continental crust (or both), or the beginning of the sea-floor spreading. Using the same notation as before, and writing μ_{Pl}, ρ_{Pl} for $T_0 < T < T_1$, and μ_1, ρ_1 for $T_1 < T \leqslant 0$, the general equations are, at $T = 0$:

$$\alpha = \alpha_0 + \mu_{Pl}(\exp(\lambda T_0) - \exp(\lambda T_1)) + \mu_1(\exp(\lambda T_1) - 1)$$

$$\beta = \beta_0 + \rho_{Pl}(\exp(\lambda' T_0) - \exp(\lambda' T_1)) + \rho_1(\exp(\lambda' T_1) - 1)$$

The linear approximation gives

$$\alpha = \alpha_0 + \lambda\mu_{Pl}T_0 + \lambda T_1(\mu_1 - \mu_{Pl}) = \alpha_{Pl} + \lambda T_1(\mu_1 - \mu_{Pl})$$

$$\beta = \beta_0 + \lambda'\rho_{Pl}T_0 + \lambda' T_1(\rho_1 - \rho_{Pl}) = \beta_{Pl} + \lambda' T_1(\rho_1 - \rho_{Pl})$$

and

$$\epsilon_{Nd}/\epsilon_{Sr} = (\mu_1 - \mu_{Pl}) \cdot A/(\rho_1 - \rho_{Pl}) \qquad (3)$$

where

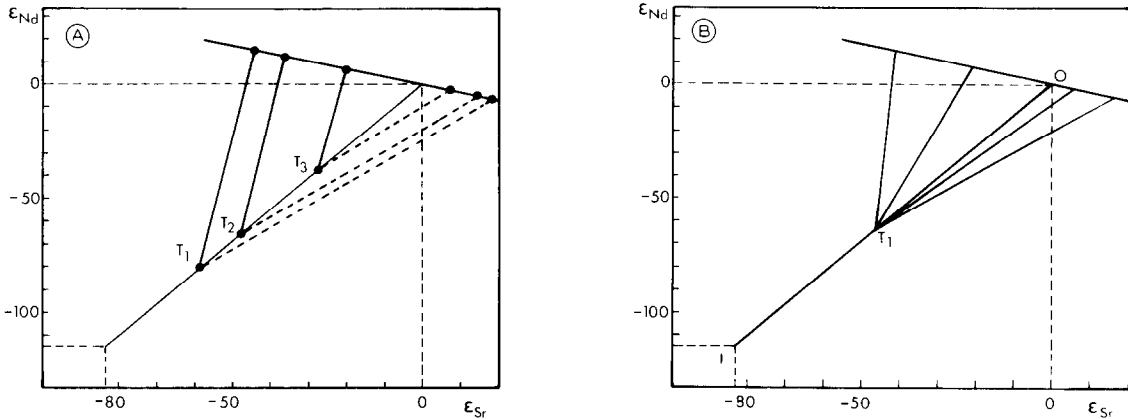$$A = \beta_{Pl}\lambda/\alpha_{Pl}\lambda' = \text{constant}$$

Fig. 4. (a) The critical model which assumes several episodes occurring at different times T_1, T_2, T_3, each having μ_2 and ρ_2 values such that $(\mu_2 - \mu_{Pl})/(\rho_2 - \rho_{Pl}) = F$ as a constant value.
(b) Model showing a large fractionation occurring at T_1, but, for each new subsystem, the fractionation law obeys the general relationship $\Delta\mu/\Delta\rho = F$. The time T_1 can be very close to the age of the Earth (e.g. 4.4 b.y.), or very late like the so-called large differentiation event at 2 b.y.

We notice that, if $(\mu_1 - \mu_{Pl})/(\rho_1 - \rho_{Pl}) = \text{constant} = \mathbf{F}$, then (3) is the equation of a line passing through the (0, 0) point, with a slope independent of T_1, the age of the fractionation event. As a consequence, if different episodes occurred at different times in the mantle, with the same fractionation law, $(\mu_1 - \mu_{Pl})/(\rho_1 - \rho_{Pl}) = \mathbf{F}$, the products of each episode measured isotopically today will have experimental points which fall on an identical line in an (ϵ_{Nd}, ϵ_{Sr}) diagram. Such an example is illustrated in Fig. 4 (a and b).

3.2.1. Consequences. Firstly, if an early differentiation event occurred at the origin of the Earth and several reservoirs were separated from each other and behaved afterwards as closed system reservoirs, this model may only give the (ϵ_{Nd}, ϵ_{Sr}) relationship previously defined if the Sm/Nd and Rb/Sr ratios of the different reservoirs follow the fractionation law defined above.

Secondly, the preceding demonstration has shown that the (ϵ_{Nd}, ϵ_{Sr}) correlation line is defined independently of T_1, the age of the fractionation event. However, the position of a given point on this line depends on T_1.

The dispersion of the experimental points on the line gives limits to the possible time of fractionation. The extreme point on the correlation diagram is defined by $(\epsilon_{Nd})^* = (\alpha_0 + \mu_{Pl}\lambda T_0)^{-1} \lambda T_1 (\mu_1 - \mu_{Pl}) 10^4$.

During fractionation, in the mantle, the minimum value of μ_1 is 0 and this gives the limiting value for T_1:

$$T_{1(min)} = 10^4 (\epsilon_{Nd})^*(\alpha_0 + \mu_{Pl}\lambda T_0)/(-\lambda\mu_{Pl})$$

and similarly for $(\epsilon_{Sr})^*$. This determination of minimum times of differentiation is performed graphically in Fig. 5.
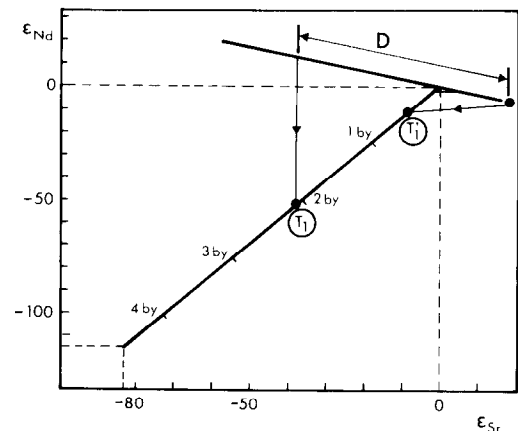

Fig. 5. The use of the spread in the data (D) to fix limitations about the time of fractionation, as explained in the text. The fractionation event certainly started before T_1 in this particular case.

3.3. Multi-episodic fractionation model

We will now consider several episodes of fractionation occurring in the mantle. Such a model is probably more realistic than the single-episode version. The general equations can be written:

$$\alpha = \alpha_0 + \lambda\mu_1(T_0 - T_1) + \lambda\mu_2(T_1 - T_2) + \lambda\mu_3(T_2 - T_3)$$
$$+ \dots + \lambda\mu_n(T_{n-1} - T_n) + \lambda\mu_{n+1}T_n$$

$$\beta = \beta_0 + \lambda'\rho_1(T_0 - T_1) + \lambda'\rho_2(T_1 - T_2)$$
$$+ \lambda'\rho_3(T_2 - T_3) + \dots + \lambda'\rho_n(T_{n-1} - T_n) + \lambda\mu_{n+1}T_n$$

Rearranging the different terms leads to the equations:

$$\alpha = \alpha_0 + \lambda\mu_1 T_0 + \lambda T_1(\mu_2 - \mu_1) + \lambda T_2(\mu_3 - \mu_2) + \dots$$
$$+ \lambda T_n(\mu_{n+1} - \mu_n)$$

$$\beta = \beta_0 + \lambda'\rho_1 T_0 + \lambda' T_1(\rho_2 - \rho_1) + \lambda' T_2(\rho_3 - \rho_2) + \dots$$
$$+ \lambda' T_n(\rho_{n+1} - \rho_n)$$

and then

$$\frac{\epsilon_{Nd}}{\epsilon_{Sr}} = \frac{[\beta_0 + \lambda'\rho_{Pl}T_0][\alpha - (\alpha_0 + \lambda\mu_{Pl}T_0)]}{[\alpha_0 + \lambda\mu_{Pl}T_0][\beta - (\beta_0 + \lambda'\rho_{Pl}T_0)]}$$

with $\mu_{Pl} = \mu_1$ and $\rho_{Pl} = \rho_1$, so that

$$\epsilon_{Nd}/\epsilon_{Sr} = A \cdot \sum_1^n (\mu_{i+1} - \mu_i) T_i / \sum_1^n (\rho_{i+1} - \rho_i) T_i$$

If, for any value of n, $(\mu_{n+1} - \mu_n)/(\rho_{n+1} - \rho_n) = F =$ constant, then this is the equation of a straight line. This simple calculation shows that the multi-episodic
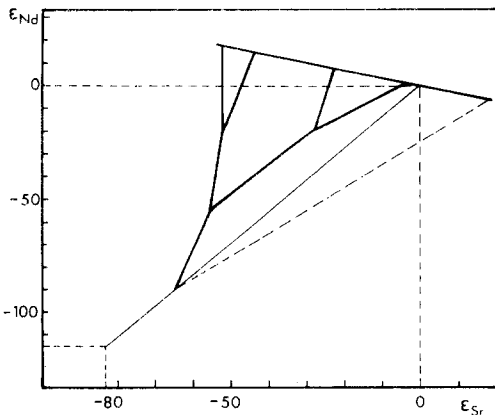

Fig. 6. Multi-episodic fractionation model, showing how the correlation line may be generated by these processes.

model gives the same relationship between ϵ_{Nd} and ϵ_{Sr} values as the single-stage fractionation process (see Fig. 6).

3.4. Mixing and multimixing

Now let us assume that the present composition is a result of mixing between two components 1 and 2 with isotopic compositions (α_1, β_1) and (α_2, β_2), and calculate the consequences of this process in the $(\epsilon_{Nd}, \epsilon_{Sr})$ diagram. If C_1, C_1' are the concentrations of Nd and Sr in component 1 and m_1 is the mass of component 1, and C_2, C_2', m_2 the concentrations and mass of component 2, and if we note that

$$a = C_1 m_1/(C_1 m_1 + C_2 m_2) = 1/[1 + (C_2 m_2/C_1 m_1)]$$

$$b = C_1' m_1/(C_1' m_1 + C_2' m_2) = 1/[1 + (C_2' m_2/C_1' m_1)]$$

we have

$$\alpha_{mix} = a\alpha_1 + (1 - a)\alpha_2 ; \quad \text{and}$$

$$\beta_{mix} = b\beta_1 + (1 - b)\beta_2$$

so that

$$(\alpha_{mix} - \alpha_2)/(\beta_{mix} - \beta_2) = (a/b)(\alpha_1 - \alpha_2)/(\beta_1 - \beta_2)$$

and

$$a/b = [1 + (C_2' m_2/C_1' m_1)]/[1 + (C_2 m_2/C_1 m_1)]$$

then if $C_2'/C_1' = C_2/C_1$, $a/b = 1$ and the mixing is represented by a straight line in the (α, β) diagram and in the $(\epsilon_{Nd}, \epsilon_{Sr})$ diagram.

In real cases C_2'/C_1', and C_2/C_1 are not too different: taking the available values for the Sr and Nd concentrations, as well as Sr and Nd isotopic ratios for the extreme oceanic basaltic rocks, we can calculate the mixing curve which is nearly a straight line (see Fig. 7a).

A second possibility is a small difference continuous mixing process. Such a mechanism will occur, for example, if during some early fractionation process, the mantle was divided into two or three reservoirs which afterwards gradually mixed. Such behaviour is the opposite of the preceding mechanism. Iteratively applying the above demonstration, it can be shown that the present $(\epsilon_{Nd}, \epsilon_{Sr})$ points will plot on a generalized mixing line.

Suppose that the Earth was differentiated into two reservoirs at time T_1. As shown before, an $\epsilon_{Nd}, \epsilon_{Sr}$ cor-
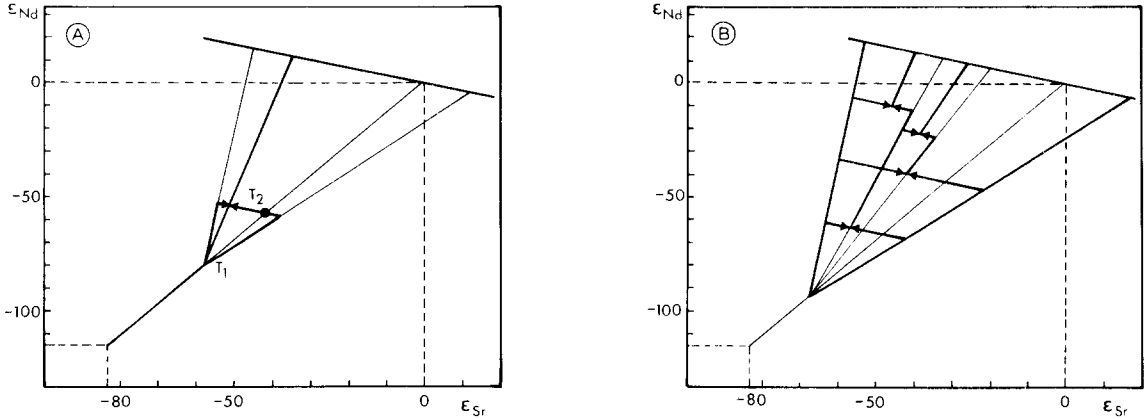
Fig. 7. (a) Mixing model between two reservoirs at T_2.
(b) Multi-mixing model, at several times between reservoirs, which follows the requirements of the fractionation laws.

relation exists if the fractionation process follows the rule:

$$(\mu_2 - \mu_1)/(\rho_2 - \rho_1) = (\mu_3 - \mu_1)/(\rho_3 - \rho_1) = \mathbf{F}$$

Then, at time T_2, we mix the two reservoirs ($a/b = 1$)

$$\alpha = \alpha_0 + \lambda\mu_1(T_0 - T_1) + \lambda(T_1 - T_2)(a\mu_2 + (1 - a)\mu_3)$$
$$+ \lambda\mu_4 T_2$$

$$\beta = \beta_0 + \lambda'\rho_1(T_0 - T_1) + \lambda'(T_1 - T_2)(b\rho_2 + (1 - b)\rho_3)$$
$$+ \lambda'\rho_4 T_2$$

taking into account that $\mu_4 = a\mu_2 + (1 - a)\mu_3$ and $\rho_4 = b\rho_2 + (1 - b)\rho_3$, we can obtain finally:

$$\frac{\epsilon_{Nd}}{\epsilon_{Sr}} = \frac{\beta_0 + \lambda'\rho_1 T_0}{\alpha_0 + \lambda\mu_1 T_0} \cdot \frac{\lambda}{\lambda'} \cdot \frac{(\mu_3 - \mu_1) + a(\mu_2 - \mu_3)}{(\rho_3 - \rho_1) + b(\rho_2 - \rho_3)}$$

(if $\rho_1 = \rho_{Pl}$, $\mu_1 = \mu_{Pl}$), so that

$$\frac{\epsilon_{Nd}}{\epsilon_{Sr}} = A \cdot \frac{(\mu_3 - \mu_1) + a(\mu_2 - \mu_3)}{(\rho_3 - \rho_1) + b(\rho_2 - \rho_3)}$$

where, as before,

$$A = \lambda(\beta_0 + \lambda'\rho_1 T_0)/\lambda'(\alpha_0 + \lambda\mu_1 T_0)$$

This calculation can be performed for other mixing stages (Fig. 7b).

3.5. General remarks about model calculations

All the models already calculated explain the (ϵ_{Nd}, ϵ_{Sr}) correlation line, and the important result

is that there is no unique solution. In particular we recall that any linear combination of the preceding models is also a solution, which adds a considerable number of further models.

4. Constraints on the evolution of the Earth's mantle

Taking the preceding models and the data published to date, we can try to deduce some constraints on the general evolution of the mantle.

4.1. Relative fractionations between Rb/Sr and Sm/Nd ratios during the major events in the mantle

As the fractionation model calculations have shown, the only simple requirement necessary to explain the (ϵ_{Nd}, ϵ_{Sr}) correlation is that:

$$(\mu_{n+1} - \mu_n)/(\rho_{n+1} - \rho_n) = F = \text{constant}$$

The experimental data permit an estimation of $\mathbf{F}$ Noting S, the slope in the (ϵ_{Nd}, ϵ_{Sr}) experimental diagram, which is given by

$$S = \mathbf{F}(\lambda\beta_{Pl})/(\lambda'\alpha_{Pl})$$

we find that $\mathbf{F} = -0.52$. With this parameter we will try to explain the observed values and then to identify the chemical process responsible for fractionation.

We consider the fractionation between stages n and ($n + 1$). If we define the enrichment factors for

302

Sm, Nd, Rb, Sr, as follows:

$$C_{n+1}^{Sm}/C_n^{Sm} = E_{(n,n+1)}^{Sm} ; \qquad C_{n+1}^{Nd}/C_n^{Nd} = E_{(n,n+1)}^{Nd} ;$$

$$C_{n+1}^{Rb}/C_n^{Rb} = E_{(n,n+1)}^{Rb} ; \qquad C_{n+1}^{Sr}/C_n^{Sr} = E_{(n,n+1)}^{Sr} ;$$

then we have

$$\mu_{n+1} = \mu_n E_{(n,n+1)}^{Sm}/E_{(n,n+1)}^{Nd} ;$$

$$\rho_{n+1} = \rho_n E_{(n,n+1)}^{Rb}/E_{(n,n+1)}^{Sr}$$

so that

$$\frac{\mu_{n+1}}{\rho_{n+1}} = \frac{E_{(n,n+1)}^{Sm} \cdot E_{(n,n+1)}^{Sr}}{E_{(n,n+1)}^{Nd} \cdot E_{(n,n+1)}^{Rb}} \cdot \frac{\mu_n}{\rho_n}$$

We know that the ratios μ_n/ρ_n vary greatly during fractionation processes because these ratios are proportional to the slopes $\lambda\mu_n/\lambda'\rho_n$ of the evolution lines in the (α, β) diagram, and the slopes are variable because there is a large variation in the observed values of $\epsilon_{Nd}, \epsilon_{Sr}$. Thus,

$$E_{(n,n+1)}^{Sm} \cdot E_{(n,n+1)}^{Sr}/E_{(n,n+1)}^{Nd} \cdot E_{(n,n+1)}^{Rb}$$

is variable.

Since $(\mu_{n+1} - \mu_n)/(\rho_{n+1} - \rho_n) = F =$ constant,

$$\frac{[E_{(n,n+1)}^{Sm}/E_{(n,n+1)}^{Nd} - 1]}{[E_{(n,n+1)}^{Rb}/E_{(n,n+1)}^{Sr} - 1]} \cdot \frac{\mu_n}{\rho_n} = \text{constant}$$

We examine this relationship with the idea that successive partial meltings are responsible for the fractionation. Using the notation $(\bar{D})$ for the mean bulk partition coefficient between residual solid and liquid for these processes, and (F) for the degree of partial melting, and remembering that the solid stays in the mantle, we can write:

$$E_{Sm}/E_{Nd} = [\bar{D}_{Sm}(\bar{D}_{Nd}(1 - F) + F)]/$$
$$[\bar{D}_{Nd}(\bar{D}_{Sm}(1 - F) + F)]$$

Then

$$E_{Sm}/E_{Nd} - 1 = [(\bar{D}_{Sm} - \bar{D}_{Nd})F]/$$
$$\bar{D}_{Nd}[\bar{D}_{Sm}(1 - F) + F]$$

We should remember that in mantle conditions $\bar{D}$ is very small for both Nd and Sm, and that F is much larger. Then

$$E_{Sm}/E_{Nd} - 1 \simeq \bar{D}_{Sm}/\bar{D}_{Nd} - 1$$

Then, applying the same reasoning to the Rb–Sr system and using the relationship that exists between μ_{n+1} and μ_n (and between ρ_{n+1} and ρ_n):

$$F = \left[\frac{(D_{Sm}/D_{Nd})^n - (D_{Sm}/D_{Nd})^{n-1}}{(D_{Rb}/D_{Sr})^n - (D_{Rb}/D_{Sr})^{n-1}}\right] \cdot \frac{\mu_1}{\rho_1}$$

Taking into account the available partition coefficients between mantle minerals and liquid, one can use the following approximations:

$$D_{Sm}/D_{Nd} = 1 + \Delta_1 ; \qquad D_{Rb}/D_{Sr} = 1 - \Delta_2 ,$$

with Δ_1 and Δ_2 positive; expanding to the first order gives:

$$F \simeq -\frac{\Delta_1}{\Delta_2} \cdot \frac{\mu_{Pl}}{\rho_{Pl}}$$

If n is large, these approximations are no longer valid. For small n, F is nearly constant and negative, and assumes a value in good agreement with that observed, namely $F = -0.52$.

4.2. Fractionation process during genesis of granites

We have just demonstrated that the observed correlation $(\epsilon_{Nd}, \epsilon_{Sr})$ in mantle materials is quantitatively compatible with a fractionation process occurring between liquid and solid material. However, it may be argued that such a correlation is geochemically trivial because certain links between Sm–Nd and Rb–Sr fractionation processes exist. As many modern studies have shown, the granite genesis involved complex phenomena including recycling of old sedimentary rocks, fluid phenomenon, mixing etc., (see Barker et al., 1975; Hart and Allègre, 1979) the formation of granites is certainly not a simple extraction of partial melting from the mantle. Using them to test the previous ideas, if the Nd–Sr ratio is a geochemical constant then the granites should
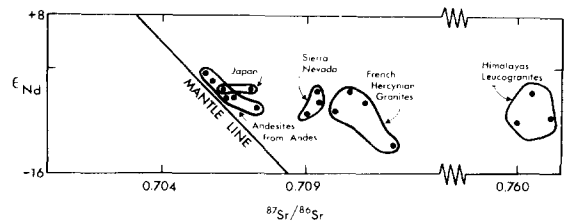

Fig. 8. Nd–Sr correlation diagram for some granites studied by Ben Othman et al. (1979).

plot on the line, but if the relationship is more specific of mantle material then they should not.

The recent studies of granites by Ben Othman et al. (1979) answer the questions. Without going into details which will be discussed elsewhere, we note the following points. All measured values are in the $(\epsilon_{Nd} < 0, \epsilon_{Sr} > 0)$ field, but out of the mantellic trend previously discussed (Fig. 8). Several trends may exist, with one particularly clear. As discussed by Ben Othman et al. (1979) such a trend implies recycling of continental crust as well as fractionation during the erosion—sedimentation cycle and thus corresponds to a very different process. But clearly these results are not similar to those for the mantle material, thereby offering a demonstration of the nontriviality of the observed Nd—Sr correlation (see Fig. 8).

4.3. Single episode or multi-episode fractionation

As we have shown in the theoretical section, the use of the $(\epsilon_{Nd}, \epsilon_{Sr})$ correlation diagram does not differentiate between single- and multiple-stage fractionation processes in the mantle during geological times. This finding is opposite to that of De Paolo and Wasserburg (1977) who used the correlation diagram to calculate an age of differentiation of the mantle. In fact, the problem is to know whether we can speak about a unique differentiation process for the earth (for example 4.2 billion years ago), or if we have continuous evolution.

This problem of "catastrophism or continuous evolution process" is an old one. We wish to discuss it here, and finally we declare our support for a continuous (but not uniform) evolution fractionation process, in opposition to the point of view popular at present.

The Alpine Lherzolites are pieces of mantle placed tectonically on the continent edge during orogenic processes (Nicolas and Jackson, 1972). This point of view is now well documented, by structural arguments (Boudier and Nicolas, 1972), by experimental petrology (Kornprobst, 1969; O'Hara, 1967), and geochemically (Loubet et al., 1975; Loubet, 1976; Frey, 1969). Geochemically, the residual character of these bodies, which are clearly situated in the family of suboceanic mantle (Richard et al., 1979), has been well documented. Therefore, this material is a piece
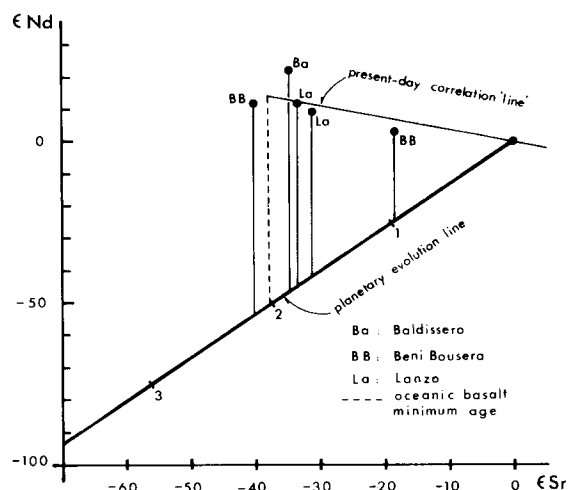

Fig. 9. Nd—Sr diagram for the orogenic Lherzolites from the work of Richard et al. (1979). The vertical lines intersect the planetary line and give the minimum times of differentiation.

of mantle for which we can obtain directly the neodymium isotopic ratios relevant to the $^{87}Sr/^{86}Sr$ and Rb/Sr ratios. It is then possible to calculate "model age" relative to the planetary evolution line. The "model age" will give the time when this part of the mantle moved out of the planetary evolution line (Fig. 9). If the fractionation episode is unique the different evolution lines will converge and then the different model ages will be identical. The Sm—Nd and Rb—Sr ages will be similar. Such studies have also been done by Richard et al. (1979) and by Polvé and Allègre (1979) and the results are clearly illustrated in Fig. 10. These bodies do not derive from a single episode. Even at the scale of one body we can detect several episodes spaced in time by several hundred millions of years. These results are in complete agreement with the detailed analysis of Loubet (1976) based on trace elements, and that of Polvé and Allègre (1979) on Rb—Sr which propose a multi-episodic history for these bodies (see Fig. 10a, b). But these bodies can be plotted on the Nd—Sr isotopic correlation diagrams and are perfectly representative of oceanic mantle in the sense of De Paolo and Wasserburg (1977). We therefore believe that such sets of observations are extremely potent arguments for the multi-episode fractionation history of the mantle.
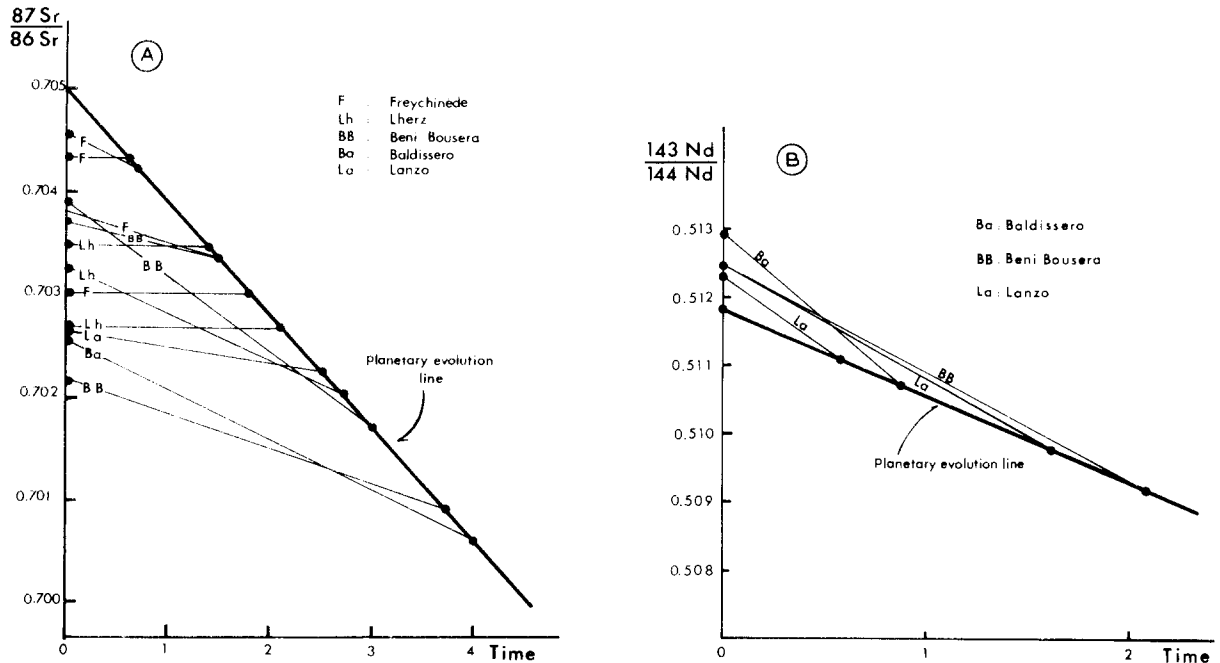
Fig. 10. (a) Strontium vs. time evolution diagram for the orogenic lherzolites. Data are those of Polvé and Allègre (1979). The line for each rock is determined by its $^{87}Sr/^{86}Sr$ and Rb/Sr ratios. The intercept with the planetary evolution line gives the "model age", as discussed in the text.

(b) Neodymium vs. time evolution diagram for the orogenic lherzolite. Data are those of Richard et al. (1979). The lines have a similar significance as noted above. We should note the variable "model age" even inside a single massif.

4.4. Constraints about the timing of the evolution of the mantle

4.4.1. Data from Alpine Lherzolites

With the data from Alpine Lherzolites we can formulate important constraints about the timing of the mantle evolution. These constraints can be derived in two ways. The first method mainly uses the $(\epsilon_{Nd}, \epsilon_{Sr})$ correlation diagram, and the second uses the evolution of Nd and Sr isotopes in the mantle controlled by the chemical fractionation factors.

(1) The methods of computing the minimum age of the beginning of fractionation have already been explained. Essentially, we draw a line parallel to the ϵ_{Nd} axis from the experimental point in the $(\epsilon_{Nd}, \epsilon_{Sr})$ diagram, and we read the minimum age from the scale on the planetary evolution line. The present available data (see Fig. 9) for orogenic lherzolites is 2.17 billion years, and for oceanic basalts is 2.0 billion years.

(2) In the second method, we note that in every liquid–solid fractionation process the liquid is enriched in Rb with respect to Sr, and in Nd with respect to Sm. The residual solid (mantle) is the end-product of this process. The result (shown in Fig. 10) is that, the minimum age of the starting of fractionation is given by the intercept of the planetary line with the present-day Sm/Nd and Rb/Sr vectors, in the diagrams (Nd isotope vs. time) and (Sr isotope vs. time), respectively. On the whole, such calculations give a minimum age of fractionation for the *oceanic* mantle of 3.1 billion years. This value seems to be in contradiction with the data obtained by De Paolo and Wasserburg (1977) and by Hamilton et al. (1977) from Precambrian volcanics and plutonic rocks. These latter data suggest that the Precambrian mantle was approximately planetary (so far as the rare-earth constituents are concerned). Our results, in contrast, suggest that the fractionation occurred very early in the Earth's history, and that the departure of the neodymium isotope from the planetary line seems to have started even earlier.

However, we do not feel that such a contradiction is too serious. Firstly, the difference in Archean between open-system and planetary closed-system $^{143}Nd/^{144}Nd$ ratios will be extremely small and not easy to detect experimentally. Secondly, the mentioned authors have studied mostly subcontinental evidence. We know however, from the work of De Paolo and Wasserburg (1977), that subcontinental present-day mantle is almost planetary but completely different from the oceanic mantle.
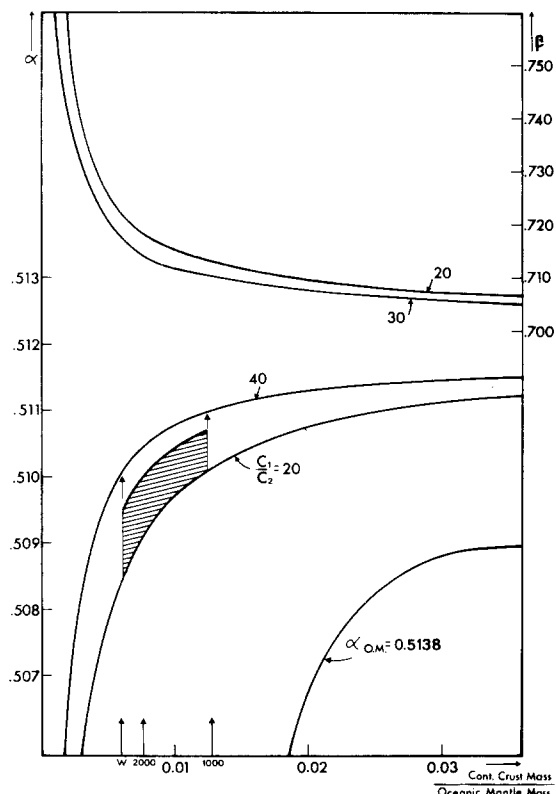

Fig. 11. Semi-quantitative mass balance between mantle and continental crust.
Mass percentage: continental crust, 0.4% Earth; whole mantle, 68% Earth.
Concentrations: Nd in continental crust, 12.6 ppm (20 times the chondritic concentration); Nd in mantle material, 0.5—0.63 ppm (0.8—1 times the Sr chondritic concentration); in continental crust, 30 ppm; Sr in mantle material, 1 ppm.
Isotopic ratios: α in oceanic mantle, 0.5122; β in oceanic mantle, 0.703; α in continental crust, 0.51181; and β in continental crust, 0.7048.
The three arrows on the horizontal axis correspond to the whole mantle, the upper mantle (2000 km), and the upper mantle (1000 km), respectively.

Therefore, for these two reasons we believe that the experimental results of De Paolo and Wasserburg (1977) and those of Hamilton et al. (1977) are not very relevant to the problem of the starting time for the open behaviour of the oceanic mantle.

4.4.2. Material balance in the oceanic mantle

The second point we wish to discuss is the material balance for the oceanic mantle. A qualitative inspection of the existing data suggest, both for strontium and neodymium, that the continental crust is the complement of the oceanic mantle. Such a claim should be checked quantitatively.

The balance equations, similar to those already discussed, are as follows:

$$\alpha_\Sigma = \alpha_{om} \cdot a + \alpha_{cc}(1 - a)$$

$$a = \left[1 + \frac{\text{Concentration in continental crust}}{\text{Concentration in oceanic mantle}} \cdot \frac{M_{cc}}{M_{om}}\right]^{-1}$$

where subscripts cc denote continental crust, and om the oceanic mantle. We can then deduce the relationship between $M_{cc}/M_{om} = x$ and the α value of the continental crust:

$$\alpha_{cc} = [(\alpha_\Sigma C_{cc}x/C_{om}) + \alpha_\Sigma - \alpha_{om}]/[xC_{cc}/C_{om}]$$

and a similar equation can be written for β. Taking C_{cc}/C_{om} for Nd over a range of 20 to 40, and using a similar range for Sr we can draw the corresponding curve (see Fig. 11 and its caption).

If we consider the whole mantle to be involved, we find values for the Nd and Sr isotopic ratios, respectively, of 0.5095 and 0.720, which are perfectly reasonable values for *mean continental crust*. For a more restricted part of the mantle the values are still reasonable, but they are certainly not valid if only a small part of the mantle is involved, because 0.5107 and 0.713 will be too different from those observed. Then the data need a complete balance between oceanic mantle and continents. A similar line of reasoning is not true for U—Pb systems, as will be discussed extensively in another paper.

5. General conclusions

We believe that we have conclusively documented the fact that the Nd—Sr isotopic correlation observed in oceanic mantle material is the consequence of:

(1) A continuous extraction of the liquid from the mantle through magmatic processes.

(2) Such a process started very early in the Earth's history.

(3) A large fraction of the mantle is involved in this process.

Such boundary conditions are in agreement with the convective-differentiation model to explain the chemical evolution of the Earth.

References

Barker, F., Wones, D.R., Sharp, W.N. and Desborough, G.A., 1975. The pines peak batholith, Colorado Front Range, and a model for the origin of the "Gabbro–Anorthosite–Syenite–Potassic" suite. Precambr. Res., 2: 97–160.

Ben Othman, D., Richard, P. and Allègre, C.J., 1978. Neodymium and strontium isotopes in granites. In preparation.

Boudier, F. and Nicolas, A., 1972. Fusion partielle gabbroïque dans la lherzolite de Lanzo (Alpes Piémontaises). Schweiz. Mineral. Petrogr. Mitt., 52: 39–56.

De Paolo, D.J. and Wasserburg, G.J., 1976a. Nd isotopic variations and petrogenetic models. Geophys. Res. Lett., 3: 249–252.

De Paolo, D.J. and Wasserburg, G.J., 1976b. Inferences about magma-sources and mantle structure from variations of ^{143}Nd/^{144}Nd. Geophys. Res. Lett., 3: 743–746.

De Paolo, D.J. and Wasserburg, G.J., 1977. The sources of island arcs as indicated by Nd and Sr isotopic studies. Geophys. Res. Lett., 4: 465–468.

Frey, F.A., 1969. Rare earth abundances in a high temperature peridotite intrusion. Geochim. Cosmochim. Acta, 33: 1429–1447.

Hamilton, P.J., O'Nions, R.K. and Evensen, N.M., 1977. Sm–Nd dating of Archean basic and ultrabasic volcanics. Earth Planet. Sci. Lett., 36: 263–268.

Hart, S.R. and Allègre, C.J., 1979. Trace-elements constraints on magma genesis. Physics of magmatic processes. Bowen Volume, Princeton University Press, Princeton, N.J.

Hawkesworth, C.J., O'Nions, R.K., Pankurst, R.J., Hamilton,
P.J. and Evensen, N.M., 1977. A geochemical study of island-arc and back-arc tholeiites from the Scotia Sea. Earth Planet. Sci. Lett., 36: 253–262.

Kornprobst, J., 1969. Le massif ultrabasique des Beni-Bousera. Etude des péridotites de haute température et haute pression et des pyroxénolites avec ou sans grenat qui leur sont associées. Contrib. Mineral. Petrol., 23: 283–322.

Loubet, M., 1976. Géochimie des Terres Rares dans les massifs de péridotites dits "de haute température". Evolution du manteau terrestre. Thèse de Doctorat d'état, Université Paris VII.

Loubet, M., Shimizu, N. and Allègre, C.J., 1975. Rare earth elements in Alpine peridotites. Contrib. Mineral. Petrol., 53: 1–12.

Lugmair, G.W., 1974. Sm–Nd ages: a new dating method (abstract). Meteoritics, 9: 369.

Lugmair, G.W., Scheinin, N.B. and Marti, K., 1975. Search for extinct ^{146}Sm. The isotopic abundance of ^{142}Nd in the Juvinas Meteorite. Earth Planet. Sci. Lett., 27: 79–84.

Lugmair, G.W., Marti, K., Kurtz, J.P. and Scheinin, N.B., 1976. History and genesis of lunar troctolite 76535, or: How old is it? Proc. Lunar Sci. Conf., 7th: 2009–2033.

Nicolas, A. and Jackson, E.D., 1972. Répartition en deux provinces des péridotites des chaînes alpines longeant la Méditerranée: implications géotectoniques. Schweiz. Mineral. Petrogr. Mitt., 52: 479–495.

O'Hara, M.J., 1967. Mineral facies in ultrabasic rocks. In: P.J. Wyllie (Editor), Ultramafic and related rocks. Wiley, New York, pp. 7–17.

O'Nions, R.K., Hamilton, P.J. and Evensen, N.M., 1977. Variations in ^{143}Nd/^{144}Nd and ^{87}Sr/^{86}Sr in oceanic islands. Earth Planet. Sci. Lett., 34: 13–22.

Polvé, M. and Allègre, C.J., 1979. ^{87}Rb–^{87}Sr systematics in orogenic lherzolites: local mantle heterogeneities, their genesis, their consequences for the basalt formation. In preparation.

Richard, P., Shimizu, N. and Allègre, C.J., 1976. ^{143}Nd/^{144}Nd, a natural tracer: an application to oceanic basalts. Earth Planet. Sci. Lett., 31: 269–278.

Richard, P., and Allègre, C.J., 1979. Origin of ophiolite complexes and orogenic lherzolite massives determined by ^{143}Nd/^{144}Nd and ^{87}Sr/^{86}Sr isotopic ratios. Eos, in press.